RESEARCH ARTICLE

Sparkling Organic Phosphorescence from Fluorinated Tetrathia[7]helicenes: Synthesis and Photophysical, Electrochemical and Computational Studies

Alberto Bossi,*[a,b] Patrizia R. Mussini,[c,b] Gianluca Farinola,[d] Marta Penconi,[a,b] Silvia Cauteruccio,[c] Mark E. Thompson,[e] Emanuela Licandro *[c,b]

[a] Dr, A. Bossi; Dr. M. Penconi;
Istituto di Scienze e Tecnologie Chimiche "Giulio Natta" (CNR-SCITEC)
Consiglio Nazionale delle Ricerche
via Fantoli 16/15, 20138 Milan, Italy
E-mail: alberto.bossi@scitec.cnr.it
Homepage: http://www.scitec.cnr.it/personale/fantoli/alberto-bossi

[b] Dr, A. Bossi, Dr. M. Penconi, Prof. P.R. Mussini, Prof. E. Licandro
SmartMatLab Center
via C. Golgi 19, 20133 Milan, Italy

[c] Prof. P.R. Mussini, Prof. S. Cauteruccio, Prof. E. Licandro
Department of Chemistry
Università degli Studi di Milano
via C. Golgi 19, 20133 Milan, Italy
E-mail:emanuela.licandro@unimi.it
Homepage: https://sites.unimi.it/licandrogroup/

[d] Prof. G. Farinola
Department of Chemistry
Università degli Studi di Bari
via Orabona 4, 70125 Bari, Italy

[e] Prof. M.E. Thompson
Department of Chemistry, Chemical Engineering and Materials Science
University of Southern California
3620 McClintock Ave, Los Angeles, California 90089-1062, USA

Supporting information for this article is given via a link at the end of the document.

Abstract: Structure-property correlations in the thiahelicene family are often not trivial since most of the functional groups present on the helical scaffold modify the conjugation size of the π-system. Selecting fluorine containing groups to provide strong inductive effects without interacting with low-lying orbitals of the system could be the way to overcome the issue. Here we report a study on three fluorine-functionalized tetrathia[7]helicenes highlighting interesting correlations between the position of the functional groups and the conjugated skeleton properties. Helicenes **Heli-F2** and **Heli-CF-F2** were prepared by photoinduced isomerization-electrocyclization (the Mallory photocyclization) of the corresponding fluorinated benzodithienyl-ethenes **Alk-F2** and **Alk-CF-F2**, which were prepared, in high yields, through stereo-conservative Stille reaction. Notably these helicenes were found to display green phosphorescence around 530–550 nm and the studies suggest an efficient spin orbit coupling mechanism in these high-energy triplet non-planar conjugated molecules. Both helicenes and their precursors were thoroughly characterized by means of optical and electrochemical measurements while DFT calculations enable to define a rationale on their structure-property correlations.

Introduction

Organic π-conjugated systems (both small molecules and polymers) and polycyclic aromatic compounds [1] have attracted great scientific and industrial interest over the last decades being a versatile class of optoelectronic materials which found widespread application in technologies such as OLEDs (organic light emitting diodes), non-linear optical devices, [2] OFETs (organic field effect transistors), [3] photodetectors and OPV (organic photovoltaics). [4] They combine optical and electrical features similar to those of semiconductors with the physical and chemical properties of organic materials. They also offer several advantages in terms of processing costs and mechanical properties. In addition, upon proper functionalization of the π-scaffold, the electronic properties and the solid-state intermolecular interactions can be tuned over a wide range. [5]
Diaryl-ethenes and the corresponding chiral helicenes [6] that can be prepared from them have received special attention. Helicenes are polycyclic aromatic molecules with nonplanar, screw-shaped, skeletons formed by *ortho*-fused aromatic or heteroaromatic rings; [6b,7] the intrinsic C_2-symmetric chiral helix endows helicenes with high optical rotations, strong circular dichroism [8] and circularly polarized luminescence. [9] These features, together with their interesting electronic properties, have encouraged their investigation and possible applications in several fields, such as in asymmetric organic- and organometallic catalysis; [10] for chiral recognition in biological applications [11-13] and chiral electroanalysis; [14] in nonlinear optics, in optoelectronics and phototransistors. [10,15] Examples of their unique features in electronics have been reported, exploiting circular-polarization induced phenomena. [16]

While carbohelicenes are composed solely of benzene rings in the backbone, heterohelicenes contain at least one heteroaromatic ring in the screw skeleton. Thia[n]helicenes [17] or aza[n]helicenes[18] are named after incorporation of at least one S or N atom, respectively, and [n] indicate the total number of rings. The presence of heteroatom(s) has a great impact on the geometric parameters and the electronic structure of the helix, affording unique functions and chiroptical response. [19] Among the heterohelicenes, tetrathia[7]helicenes feature seven condensed rings, four of which are thiophenes and three are benzenes. The helical pitch spans over a wide range of values enabling this framework to accommodate a large variety of even sterically demanding groups. [20]

In this frame, the knowledge and understanding of the correlations between structure, conjugation and effect of functionalization is of paramount importance for any practical exploitation. Although several functional groups, such as CHO, COOR, CN and others, have been inserted in the thiahelicene scaffold, [21] and the properties of the corresponding derivative studied, all these groups alter the size of the helical π-system as the result of an extension of the delocalization over the functional group itself. This fact could shift and blur the intrinsic helicene electronic features and electronic localization/delocalization.

In contrast, fluorination (replacement of hydrogen atoms in C-H bonds with fluorine atoms making stronger bonds) does not alter the conjugation size of molecules and has been used to switch *p*-type organic semiconductors into *n*-type one. [22] It proved to effectively tune and/or improve the properties of many classes of conjugated materials. [23] Selective fluorination of molecular structures often leads to deep changes in their physical and chemical properties and/or confers new functional properties, including *e.g.,* high thermal and oxidative stability, enhanced hydrophobicity, specific F···H–C intermolecular interactions and an inverted charge density distribution in fluoro-aromatic compounds. [24,25]

Most important, the strong inductive effect and the negligible π-donor ability of F atoms on a conjugated system can serve in the specific case in which and electronic perturbation of a conjugate system is desirable without affecting the π-size of the molecule. [26] We previously reported on the investigation of both fluorine-free and fluorine-based 1,2- bis(benzo[1,2b;4,3b']dithiophenyl)-ethenes (**Alk**s) systems both as the molecular precursors of the corresponding tetrathia[7]helicenes (**Heli**s) and as fluorophores in organic semiconductors and OLEDs. [28] Besides, a few examples of selectively fluorinated carbo [4]-,[17] [5]-,[18] [6]-,[19] and [7]-[20] helicenes have been reported in the literature.

In this work, aiming to systematically explore the electronic properties of tetrathia[7]helicenes, we have studied two series of fluorinated systems (**Heli-F2**, **Heli-CF**, **Heli-CF-F2 and Alk-F2**, **Alk-CF**, **Alk-CF-F2**, Schemes 1 and 2), in comparison with the two parent unsubstituted molecules, **Heli-H** and **Alk-H** as benchmarks, together with the known alkyl substituted **Heli-C3** and **Alk-C3**. Our designed structures feature either perfluoro alkyl chains (herein indicated as the -CF group) as functional groups at the α- position of terminal thiophene rings, and/or fluorine atoms (herein indicated as -F) bound on the ethene double bond in **Alk** and on the 7,8 positions of the helicene backbone. Both -CF and -F substituents do not change the size and extension of the conjugated scaffold in either **Alk** or **Heli**, thus allowing for a significative systematic comparison of electronic perturbations.

Here we also describe the synthesis of new molecules **Alk-F2**, **Alk-CF-F2**, **Heli-F2**, **Heli-CF-F2**, complemented by detailed photophysical and electrochemical studies also supported by DFT and TDDFT calculations.

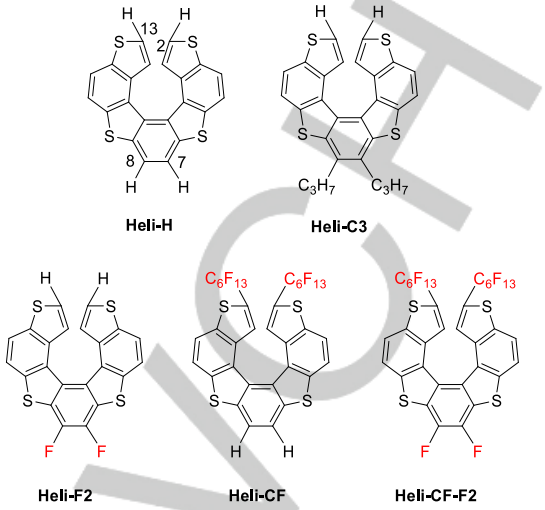

Scheme 1: Structures of the investigated tetrathia[7]helicenes, **Heli**s.

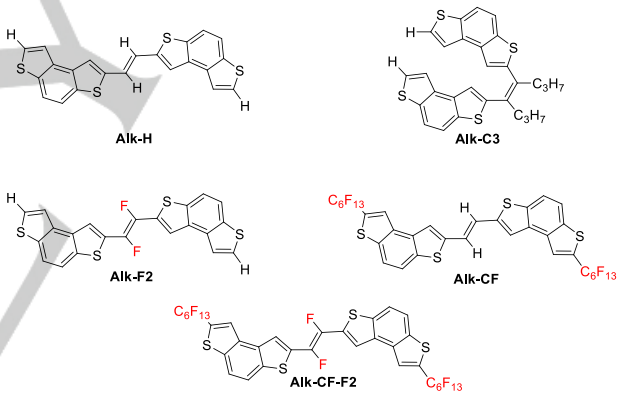

Scheme 2: Structures of the investigated bis(benzodithiophenyl)-ethenes, **Alk**s.

Results and Discussion

Synthesis

Tetrathia[7]helicenes are commonly synthesized by a photochemically promoted electrocyclization starting from 1,2-diarylethene precursors. Therefore, to obtain **Heli-F2 and Heli-CF-F2** the proper 1,2-difluoroethene precursors **Alk-F2** and **Alk-CF-F2** were prepared through a two-step procedure including the stereo-conservative Stille cross-coupling (Scheme 3) of **2a** and **2b** with the (*E*)-difluorodistannylethene (**3**) followed by the photochemically induced electrocyclization reaction (Scheme 4). In detail, the synthesis of the aryl iodide **2b** was accomplished starting from **1b** [27] employing the synthetic approach previously reported for the preparation of **2a**. [28]

Alk-F2 and **Alk-CF-F2** have been synthesized, by reacting the (*E*)-difluorodistannylethene (**3**) with two equiv. of the iodo-benzodithiophene **2a** and **2b**, respectively, in a THF/DMF solution and using $Pd(PPh_3)_4$ as catalyst in the presence of CuI (Scheme 3). [29] **Alk-F2** (83% yield) and **Alk-CF-F2** (84% yield), precipitate from the reaction mixture thus simplifying the isolation procedure which hence consists in a filtration and repeated washes with *n*-hexane.

The two yellowish solid products are barely soluble in organic solvents as previously reported for other *E*-diarylethene systems given their flat structure that induce strong π-π intermolecular interactions. [21c,28]

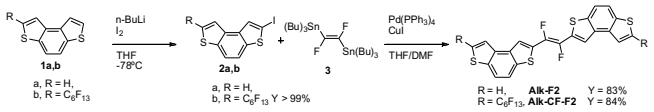

Scheme 3. synthetic procedure for the preparation of **Alk-F2** and **Alk-CF-F2**.

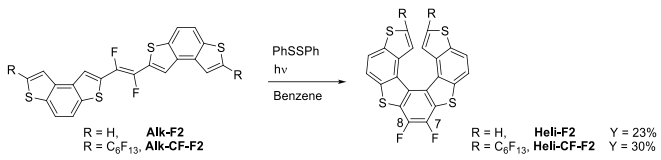

Scheme 4. photochemical cyclization procedure for the synthesis **Heli-F2** and **Heli-CF-F2**.

Helicenes **Heli-F2** and **Heli-CF-F2** were prepared by photochemical electrocyclization [30] starting from the corresponding **Alk-F2** and **Alk-CF-F2** precursors **(**Scheme 4). **Alk-F2** and **Alk-CF-F2** were suspended or dissolved, respectively, in benzene and a catalytic amount of PhSSPh was added;[31] the mixtures were irradiated, in a 250 mL photo-reactor equipped with an immersion, quartz-coated, 125W medium-pressure mercury lamp for about 8 hours until disappearance of the starting reagent. The reaction proceeded with comparable or slightly lower rate with respect to that of the *E*-**Alk-H**[21c] while resulted much slower compared to the rapid photocyclization of *Z*-**Alk-C3** to **Heli-C3**. [21b,28]

The crude mixtures were purified by column chromatography on silica gel affording pure **Heli-F2** and **Heli-CF-F2** in 23 and 30 % yields respectively. In addition, some decomposition tars eluted with methanol and difficult to characterize were obtained.

As well known, the photocyclization reaction[32] implies an *E* to *Z* isomerization of the double bond in the excited state, followed by electrocyclization and oxidation to the final helicene structure. Therefore, the formation of the target **Heli-F2** and **Heli-CF-F2** implies that *E* to *Z* photoisomerization of difluoro ethenes **Alk-F2** and **Alk-CF-F2** occurred, although this process has hardly been reported so far. [33]

Electronic spectroscopy

*1 Optical absorption and photoluminescence properties of **Alk**s.* Figure 1a shows the absorption spectra, in CH_2Cl_2 solutions, of all the alkenes; for sake of comparison the absorption of the parent benzodithiophene (**BDT**) is also included. **Alk-C3** is the only member of the series in *Z* configuration and displays a peculiar behaviour with a broad featureless absorption between 280 and 350 nm which can be related to typical non-rigid structures with sterically demanding groups; [34] it is bathochromically shifted of ca 30 nm with respect to **BDT** and its absorption locates over 80 nm higher in energy with respect to the other group members. This indicates that, in the *Z*-configuration, the conjugation extends through the ethene bond beyond the **BDT** moiety but is not effective to warrant the full communication between the two **BDT** units. All the alkenes in *E*-configuration are characterized by a highly structured absorption band between 350 and 450 nm and molar absorptivity ranging from 4×10^4 to 5.3×10^4 $cm^{-1}M^{-1}$.

Alk-H can be regarded as the reference alkene in the *E*-series allowing to monitor the electronic perturbations induced by the substituents. **Alk-H** spectrum is characterized by four clearly resolved peaks (like those of **BDT**), spaced by 1400-1500 cm^{-1}, between 330 and 420 nm (λ_{max} = 416 nm, ε_{max} = 5.3×10^4 cm^{-1} M^{-1}). The almost 100 nm redshift with respect to **BDT** and **Alk-C3** indicates an efficient conjugation extending over the two **BDT** moieties through the *E*-ethene bridge as also observed in the SI DFT section. The fluorination of the double bond in **Alk-F2** (λ_{max} = 411 nm) slightly blue-shifts the absorption by 5 nm with respect to **Alk-H**, whereas a red-shift is observed upon introduction of the perfluorohexyl chains (-CF) in **Alk-CF** (λ_{max}= 419 nm). The absorption of **Alk-CF-F2** (λ_{max}= 413 nm), which has both a fluorinated ethylene bridge and perfluoroalkyl chains, lies between that of **Alk-F2** and **Alk-CF**.

Figures 2 and S1 show the emission and excitation profiles of **Alk**s at RT and 77K; Table 1 summarizes the major photophysical parameters.

All the *E*-alkenes show structured emissions (with vibronic breathing mode of ca. 1500-1600 cm^{-1}) which mirror the absorption profiles; small or negligible Stoke shift characterizes **Alk**s emissions in both RT and 77K experiments; together with very small rigidochromic shift (see Table 1), the data are indicative of the rigid molecular framework and the strong coupling of ground (S_0) and excited (S_1) states. **Alk-CF** and **Alk-H** feature the highest fluorescence quantum yields (QY, respectively 0.53 and 0.41) while fluorination of the double bond leads to a consistent decrease in QY (0.26 for **Alk-F2** and 0.11 for **Alk-CF-F2**). All *E*-alkenes display fast fluorescence lifetimes in the nano- and sub-nanosecond scale fitted with a biexponential function indicating the presence of at least two competitive deactivations processes. Those include *E/Z* isomerization and the S_1 to T_1 intersystem crossing facilitated by the presence of the thienyl moieties. [35]

Instead, **Alk-C3**, given its Z-configuration, efficiently and quickly converts into **Heli-C3** [21b,28] in diluted solution at RT along the excitation beam path of the Xe lamp (see Figure S1, $\lambda_{exc.}$ = 350 nm, the excitation and emission profiles recorded for **Alk-C3** match those of **Heli-C3**). On the contrary, in the rigid 2MeTHF matrix at 77K, photoisomerization-cyclization no longer occurs, and the molecule displays its real broad unstructured emission in the 370-600 nm range (Figure 2c).

*2 Optical absorption and photoluminescence properties of helicenes (**Helis**).* Figure 1b reports the molar absorptivity spectra of the helicenes and Figure 1c shows a comparison between **BDT**, **Alk-H** and **Heli-H**.

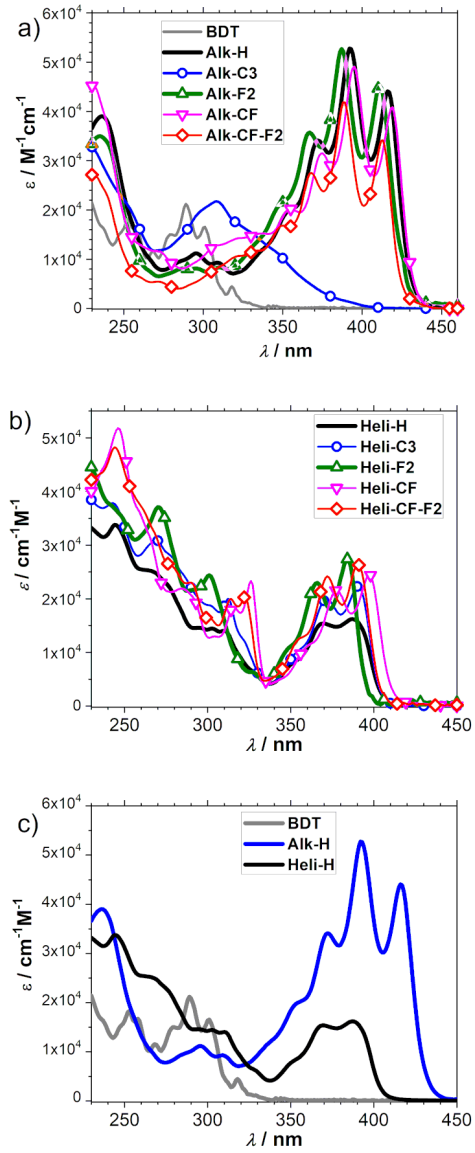

Figure 1. Molar absorptivity of a) **Alk**s; b) **Heli**s in CH_2Cl_2 solution; c) comparison of optical absorptions of BDT, **Alk-H** and **Heli-H**.

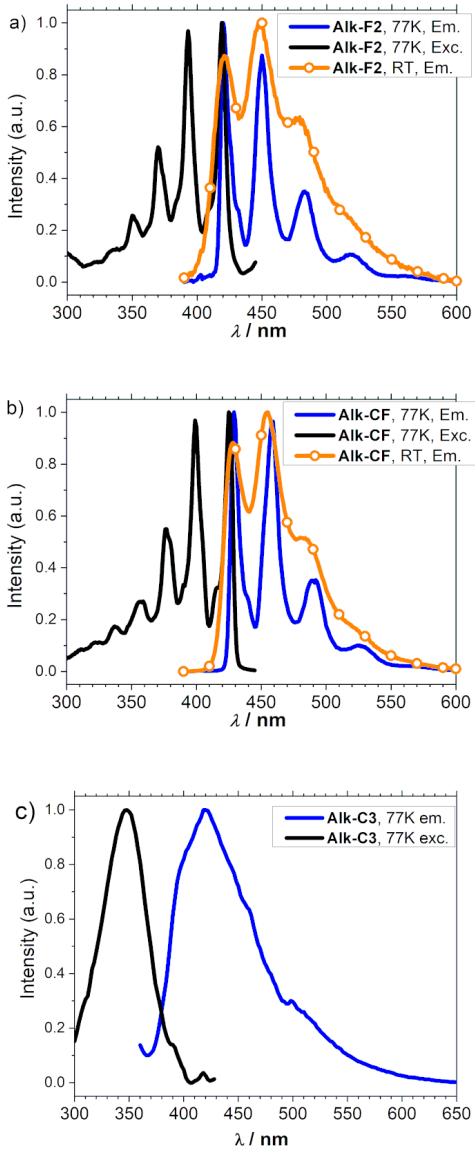

Figure 2. Excitation and emission spectra of a) **Alk-F2** and b) **Alk-CF** and c) **Alk-C3**; 77K, 2MeTHF frozen glass; RT, CH_2Cl_2 diluted solution.

Table 1. Photophysical properties of **Alk**s (CH_2Cl_2, room temperature; 2MeTHF, 77K), τ_{ave}, average lifetime in case of multiexponential decay fits

	Room temperature (CH_2Cl_2)				77K (2MeTHF)	
Compound	λ_{abs} (nm)	λ_{em} (nm)	QY	τ_{ave} (ns)	λ_{em} (nm)	τ_{ave} (ns)
Alk-C3	310	/	(0.01)		430	0.74
Alk-H	416	428	0.41	0.75	427	0.90
Alk-CF	419	429	0.53	0.77	429	0.92
Alk-F2	411	421	0.26	1.13	420	0.84
Alk-CF-F2	413	422	0.11	0.59	421	0.77

All helicenes show two distinct set of absorptions; the first one, with molar absorptivity ranging from 1.6×10^4 to 2.7×10^4 cm^{-1} M^{-1}, is located between 350–420 nm and consists of two main vibrational progression and a slightly resolved shoulder at shorter wavelength. The second set of transitions are located below 340 nm.

In analogy to the **Alk** series, **Heli-H** is taken as the reference compound for the analysis of the functionalization effects as well as for the effect of benzannulation with respect to **Alk**s. [19,36] The low energy band, which correlates to transition of HOMO to LUMO character, is particularly helpful for the understanding of the electronic perturbations of the helical system deriving from fluorination, either on the central benzene or on the terminal thiophene (see Scheme 3). When two fluorine atoms are present on the central benzene ring in the 7,8 positions (**Heli-F2**, λ_{max}= 383 nm), the absorption maximum slightly blue-shifts by 4 nm with respect to the unsubstituted **Heli-H** (λ_{max}= 387 nm).

Table 2. Photophysical parameters of **Heli**s in CH_2Cl_2 at room temperature and in 2MeTHF at 77K. λ_f refers to the maximum of the fluorescent emission; λ_p refers to the highest energy peak of phosphorescence; singlet-triplet gap S_1-T_1 calculated as the difference between λ_f - λ_p (cm^{-1}); Huang-Rhys parameter, S, calculated as the intensity ratio between the first two vibronic satellites I_1/I_0 of phosphorescence (P) and fluorescence (F); τ_{ave}, ave indicate the average lifetime in presence of multiexponential decays

	Room temperature (CH_2Cl_2)				77K (2MeTHF)						
Compound	λ_{abs} (nm)	λ_f (nm)	QY	τ_f (ns)	λ_{em} (nm)	τ_{ave} (ns)	λ_p (nm)	τ_p (ms)	S_1-T_1 (cm^{-1})	F/P ratio[c]	S
Heli-H	387	403	0.06	0.74	396	1.11	530 515 [a]	124	6385 5835 [b]	0.55	0.57(F) 1.36(P)
Heli-C3	390	401	0.10	0.88	395	1.20	543 520 [a]	137	6830 6090 [b]	0.93	0.64(F) 1.32(P)
Heli-CF	397	408	0.06	0.67	404	0.93	535 526 [a]	105	6042 5740 [b]	0.70	0.67(F) 1.18(P)
Heli-F2	383	393	0.09	0.58	389	0.90	550 524 [a]	121	7530 6625 [b]	2.61	0.74(F) 1.24(P)
Heli-CF-F2	390	401	0.10	0.56	399	0.97	555 524 [a]	92	7040 5975 [b]	1.90	0.75(F) 1.22(P)

[a] refers to the wavelength (onset criterion) corresponding to the 5% intensity of the phosphorescent emission λ_p; [b] gap calculated using the λ_p onset criterion. [c] Calculated from the integrated area of the fluorescence (F) and phosphorescence (P) at 77K (Figures 3 and S2b)

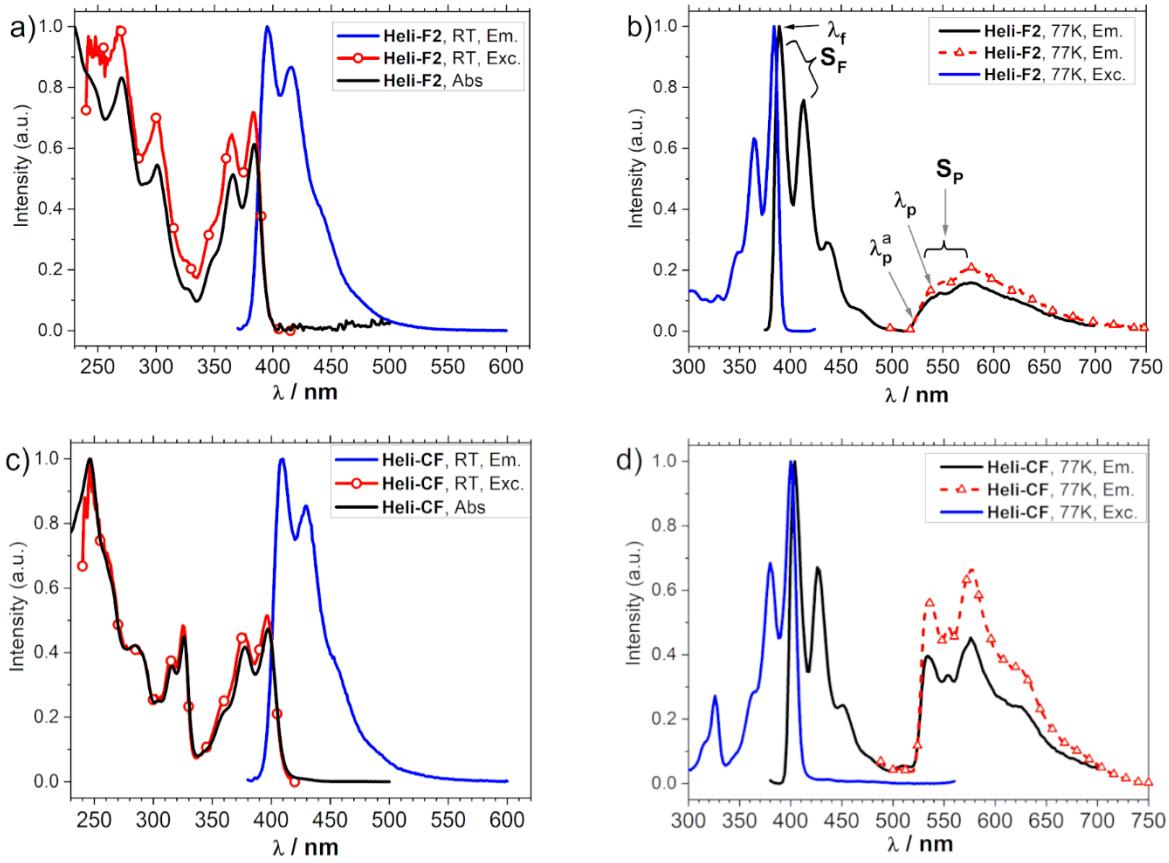

Figure 3. Absorption, excitation, and emission spectra of **Heli-F2** and **Heli-CF** (RT, CH_2Cl_2 solution; 77K, 2MeTHF frozen glass); S_F, S_P, λ_f, λ_p, λ_p^a reported in panel b) are described in the footnote of Table 2.

On the contrary, the slight donating character of alkyl groups in **Heli-C3** (λ_{max}= 390 nm) results in a slightly red-shift of 3 nm with respect to **Heli-H**.

In **Heli-CF** (λ_{max}= 397 nm), the functionalization on the positions 2,13 of terminal thiophene rings with perfluoro alkyl chains, produces a 10 nm red-shift in comparison to the parent **Heli-H**. When both perfluoroalkyl chains and fluorine atoms are present as in **Heli-CF-F2**, the absorption maximum at 390 nm is the result of a combination of the opposite effects of the substituents.

CF groups, beside the observed small bathochromic shift above 350 nm, are also responsible for a significant spectral modification at higher energy. In fact, below 270 nm **Heli-CF** and **Heli-CF-F2** display an intense transition (not present in the **Heli-H** and **Heli-C3** systems), likewise a well resolved band, consisting of two peaks, appears at 310-330 nm (Figure 1b).

Absorption profiles provide a quite useful tool to evaluate the effect of torsion/annulation on the effective conjugation (*i.e.*, optical bandgap). [37] Comparing the absorption of each **Alk** with the corresponding **Heli** derivative (see Figure 1c for **Heli-H** and **Alk-H**) we observe, on average, a 25-30 nm blue-shift (*e.g.*, λ_{max} = 411 nm in **Alk-F2** and λ_{max} = 383 nm in **Heli-F2**) suggesting that ortho-benzannulation and helical torsion result in a decrease of the conjugation.

Figure 3 reports the photoluminescence spectra of the **Heli-F2** and **Heli-CF** in CH_2Cl_2 at RT and in rigid 2MeTHF matrix at 77K, while in Figure S2 are reported all the helicenes studied. The data are summarised in Table 2.

At room temperature, in fluid solution, all the helicenes display structured fluorescence, featuring two peaks around 400 nm, whose excitation spectra perfectly overlap the UV-Vis ones; although the Stokes shifts in the range of 10 nm are signature of the π-π^* nature of the involved transition, the emissions are somehow less resolved compared to the case of the precursors **Alk**s, pointing to a less rigid framework (see below). Fluorescence QY for the studied molecules range from 0.06 to 0.10 and radiative lifetimes are in the sub-nanosecond regime. These values are similar and even higher compared to helicenes with analogous size such as carbohelicene. [38] Once doped in a rigid matrix of PMMA (2% w/w) on quartz substrate, helicenes retain their fluorescence QYs in air (ranging 0.06-0.07) with only small variation with respect to the solutions; these data and the collected photophysical parameters of PMMA films are reported and summarised in Table S1.

At 77K in rigid matrix, the fluorescence emission undergoes a small rigidochromic blue shift and gains a more pronounced structure featuring three peaks spaced by ca 1350-1450 cm^{-1}, as evident from Figure 3. Therefore, in the rigid matrix some distortions and vibrational coupling modes between the involved transition states are silenced (i.e., helical pitching).

The most important feature that emerges from the low temperature investigation relates to the emission bands between 520 and 700 nm (Figures 3 and S2). These bands display some vibronic features and are characterized by relatively long radiative lifetime in the range of 80–150 ms (Table 2). At room temperature, this long wavelength photoluminescence was not observed in solution, but it is clearly visible once helicenes are casted as thin film embedded into PMMA matrix (Figure S2c). The photoluminescence experiments, conducted on the PMMA doped film in air and nitrogen saturated environment (or high vacuum evacuated Schlenk tube), unambiguously demonstrate the oxygen quenching effect on the 520–700nm emission. The presence and formation of either ground state dimeric aggregates or excimers as the origin of these bands can be excluded given: (a) the low chromophore concentration in the 2MeTHF matrix as well as in the PMMA film, (b) the nearly identical UV excitation profile matching the solution absorption, and (c) the absence of raise time component in the long wavelength emission.

Therefore, the emissions between 520–700 nm can be attributed to the phosphorescence of the thiahelicenes, [39] a phenomenon that, to the best of our knowledge, has never been deeply surveyed in tetrathia[7]helicenes except for a recent report on gold phosphanes. [40]

Phosphorescence results from the fast intersystem crossing (ISC) of the lowest excited S_1 state into the triplet T_1 one[41] followed by radiative T_1 - S_0 transition. In fact, the excitation spectra measured for the fluorescence (S_1 - S_0) and for the phosphorescence transitions perfectly match each other. The related ISC and phosphorescence processes in this type of structure arises from two different contributions: the non-planar helically twisted structures which has been proved to be responsible of ISC enhancement and the presence of sulphur heteroatoms along the conjugated system that can significantly enhance ISC through the introduction of low-lying *n* - π^* states (involving the lone pairs on the thiophene atom) that couple to the π - π^* states of triplet multiplicity. [42]

3 Photophysics of the T_1 state. [43] Considering the size of the π-system of helicenes, featuring seven ortho-condensed aromatic rings, the T_1 state locates on average at quite high energy, ca 520–550 nm (18000–19000 cm^{-1}). As references, naphthalene (two condensed rings) has its triplet emission located at 21200 cm^{-1}, phenanthrene (three ortho-condensed rings) at 21730 cm^{-1}, anthracene (three para-condensed rings) at 14927 cm^{-1} and benzophenanthrene (four ortho-condensed rings) at 20020 cm^{-1}. [44]

The triplet lifetimes (τ_p, table 2) are noticeable short (ca. 0.1 s) compared to that typical of most organic molecules (τ_p of ca. 1 to 10 s). Likewise, lifetimes are nearly one order of magnitude shorter in tetrathia[7]helicenes than in carbohelicene and azahelicene systems in similar conditions. [39,42,45] Such significant shortening underlines that the triplet-to-singlet transitions, both radiative and non-radiative, are significantly allowed in thiahelicenes and therefore spin-orbit coupling (SOC) [46] is quite efficient.

In this helicene series, the singlet-triplet gap (S_1-T_1), as the energy difference between the 0-0 fluorescence peak and the phosphorescence onset (defined herein as the wavelength $\lambda_p{}^a$ whose phosphorescent intensity is 5% of the λ_p one, Figure 3b) ranges from 5700 to 6600 cm^{-1}. This gap is interestingly small, somehow comparable to the S_1-T_1 gap of phenanthrene-like molecules, and, together with the short lifetime, is one of the origins of the remarkable high phosphorescence intensity. [44] Interestingly, the ratio between the fluorescence and the phosphorescence integrated areas (F/P, Table 2) is smaller than 1 for **Heli-CF** and **Heli-H** (being respectively 0.7 and 0.55), approaches unit in **Heli-C3** and, in the fluorine substituted systems significantly increases being 1.9 in **Heli-CF-F2** and 2.6 in **Heli-F2** (Table 2).

Heli-CF is the only helicene featuring a well resolved triplet emission while the other systems are characterized by three broad peaks which smear one over the other in the 7,8 F-substituted helicenes.

Most polycyclic aromatic systems, characterized by planar extended structures (*e.g.,* naphthalene, anthracene, phenanthrene, triphenylene) display structured fluorescence as well as phosphorescence at 77 K in rigid matrix with the typical 1400–1500 cm^{-1} peak breathing. [47] Therefore, parameters other than C-C and C-H vibrations must be considered for helicenes to shed light on their phosphorescence. Unfortunately, there is not such an extended literature data concerning these studies on helical systems. According to some literature references, [45] the shape of the T_1 emission is the result of vibration and breathing of the helical motif in the triplet state (i.e., changes in the helical pitch). In fact, the millisecond phosphorescence decay regime would allow helix breathing modes which, by geometry rearrangements (see Huang-Rhys parameter below), broaden the vibronic satellites.

An evaluation of such modes can be performed from the analysis of the Huang-Rhys parameter, S (calculated as the intensity ratio between the first two vibronic satellites I_1/I_0 of each band). Since S is proportional to the coordinate displacement, $(\Delta Q)^2$, of the two potential energy surfaces involved in the emission process (S_0 and T_1 in the present situation), an S parameter <1 indicates that vertical transitions occur between similar potential surface coordinate (and therefore similar geometry of the involved states); on the contrary, as S become larger (>1), the two potential surfaces are displaced (by a ΔQ) and therefore the excited and ground state geometries substantially differ. In the studied helicenes, S_P ranges between 1.18 to 1.36, therefore suggesting a significant geometry distortion of the T_1 state. In contrast the S_1 states originating the fluorescent signals are all characterized by S_F largely < 1.

Electrochemical characterization*:*

The redox properties of fluorinated tetrathia[7]helicenes **Heli-CF**, **Heli-F2**, and **Heli-CF-F2** have been investigated by cyclic voltammetry (CV) in CH_2Cl_2 (granting excellent solubility for all compounds) and in acetonitrile (ACN), because of the larger window of available potentials for reductions, and therefore affording better resolution of the reduction peaks located at the most negative potentials.

Heli-H and **Heli-C3** have been included as non-fluorinated benchmarks for **Heli-F2** and **Heli-CF-F2** concerning 7,8 - positions.[36] Due to the lower solubility of **Heli-C3** and **Heli-CF** in ACN, the mixture ACN/toluene 1:4 was employed, thus improving their solubility while still granting a significant amount of polar and coordinating ACN solvent. It must be remarked that, on account of the different polarity and coordination ability of CH_2Cl_2 and ACN, differences in CV patterns can be observed even after normalization against the $Fc^+|Fc$ intersolvental reference couple, pointing to solvent effects in the electron transfer processes and on subsequent chemical steps.

A synopsis of normalized CV features is provided in Figures 4 (CH_2Cl_2) and Figure S15 (ACN or ACN/toluene); key parameters are summarized in Table 3 while full CV data are reported in Table S3.

Heli-H and **Heli-C3** feature a chemically irreversible first oxidation peak, corresponding to a complex process including more than one electron transfer step (by comparison with the first reduction peak considering the CV patterns in ACN reported in the SI) and one or more chemical steps; this can be ascribed to the formation of a radical cation mainly localized in the α positions of the thiophene terminals on account of the tendency of the molecules to electro-oligomerize as previously described.[36] The electron donating effect of the alkyl chains in **Heli-C3** respect to **Heli-H** should result in a negative shift of both first oxidation and first reduction potential respect to **Heli-H**; however, a significant shift by ca. 100 mV is observed for the reduction potential, while it is nearly unperceivable in the oxidation case. A possible explanation could be in terms of an additional effect related to the steric hindrance of the alkyl chains, which could hamper first oxidation, resulting in a positive potential shift contribution, and likely also first reduction, resulting in a negative potential shift contribution. It must be however underlined that both inductive and steric hindrance effects could be of different extent for first oxidation and first reduction if the corresponding active sites have significantly different location on the conjugated system.

Changing the weakly electron donating propyl chains in positions 7,8 with two strongly electron accepting fluoride atoms (**Heli-F2**) results in a significant shift of both first oxidation and first reduction potential in the positive direction. (Figures 4 and S15, Table 3). This shift is slightly (CH_2Cl_2) or significantly (ACN) higher for the reduction peak than for the positive one, which might point out, like in the above benchmark case, to the radical anion and radical cation to be somehow differently localized in the aromatic system. In particular, the radical cation might be localized somehow farer away from the 7,8 positions, which is also in agreement with the radical cation coupling process on the α-thiophene terminals formerly observed in several thiahelicenes, [36] However, while **Heli-C3** was able to oligomerize, albeit much slower than **Heli-H**, **Heli-F2** is not; therefore, fluorine atoms hamper oligomerization more than propyl chains on the same 7,8 positions.

Focusing on the **Heli-F2** first reduction process, it is accounted for by a monoelectronic peak in ACN (similarly to **Heli-C3**); such peak appears chemically irreversible at 0.2 V/s scan rate but gradually becomes chemically reversible with increasing scan rate, pointing to formation of a radical anion undergoing a subsequent chemical step of moderate rate constant, appreciable in the experiment timescale range. Moreover, a second monoelectronic reduction peak, close to the first one and tending to reversibility with increasing scan rate, can be perceived for **Heli-F2** unlike **Heli-C3** (on account of the above-mentioned inductive effect resulting in a positive shift of all signals). Globally considering such twin-peak first reduction system, it could account for two equivalent, reciprocal interacting redox site moieties.

Functionalization of the 2,13-thiophene positions with perfluorinated chains results in an even stronger positive shift on the first oxidation potential of **Heli-CF** than the one observed in **Heli-F2**. This can be justified in terms of both the strong electron attracting inductive effect[48] and the steric hindrance effect of the perfluorinated chains bound to the α positions of the terminal thiophene rings. Each perfluorinated chain linked to the π system provides, in addition, a new electrochemically reactive group in the investigated potential range. In fact, the huge reduction peak observed at much more positive potentials than the one localized on the tetrathiahelicene system in **Heli-F2**, should account for a complex, multielectronic process which, according to Uneyama *et.al.*, [49] can be associated to reductive C–F cleavage on the perfluorinated chains, initiated by electron uptake by the adjacent π system (electroreductive cleavage of simple perfluoroalkyl chains do take place, but at much more negative potentials). [50]

It is also interesting to compare the CV pattern of **Heli-CF** with that **Alk-CF** (Figure S15a). While the first reduction process related to the perfluoroalkyl chains practically coincides for the two molecules, this is not true for the first oxidation process, involving the conjugated backbone. In the case of **Alk-CF,** oxidation is located at less positive potentials respect to **Heli-CF**, which looks consistent with the above discussed better conjugation efficiency of the quasi-planar system respect to the helical one, in spite of the latter featuring an additional aromatic ring, which however looks of negligible effect on the global conjugation (actually, in thiahelicene systems alternating benzene and thiophene rings, electronic properties are mostly determined by the thiahelicene rings) while more determining appears the loss of planarity. Notably, in the **Alk** case first oxidation peak is monoelectronic and chemically and electrochemically reversible, pointing to facile electron transfer to the π system and to the formation of a stable radical cation, which is consistent with the terminal positions being capped by the perfluoroalkyl chains (which should also favour localization of the radical cation rather on the middle than on the terminals of the aromatic system). Moreover, a first oxidation two-peak system is observed, which could correspond, once more, to the oxidation of two equivalent, reciprocally interacting redox centres, corresponding to the two benzodithiophene units communicating through the central double bond.

Finally, **Heli-CF-F2** combines the features of **Heli-CF** and **Heli-F2**. Its reduction peak coincides with the **Heli-CF** since it is determined and localized on the perfluoroalkyl chains; its oxidation peak is displaced at very positive potentials, as a consequence of the inductive effects of both the F atoms on the 7,8-positions and the perfluoroalkyl groups on the 2,13-ones, as well as, possibly, also of their steric hindrance). Even for this molecule, as for the former ones, no significant deposition of a conducting film was observed, in accordance with the thiophene terminals being capped.

Theoretical calculations.

Ground state geometries of the **Heli** and **Alk** systems were optimized by DFT BL3YP/6-31G* theory level which was shown to provide good consistency with experimental X-ray parameters as previously reported. [51] The first six excited states (both singlet and triplet) were calculated by TD-DFT BL3YP/6-311G*.[51] The main data on **Heli**s are collected in table 4 (extended data and those of **Alk**s see the DFT section in the supporting information, table S4) and the calculated vertical, Frank-Condon, transitions are found to nicely reproduce the experimental trend for the two class of molecules. [52]

Together with the singlet ground state, optimized triplet states were also calculated for the helicene group. As the result of DFT and TDDFT calculations, compared to reference **Heli-H** (λ_{calc} = 385nm), **Heli-CF** (λ_{calc} = 395nm) display a red-shifted absorption, whereas **Heli-F2** (λ_{calc} = 384nm) is only slightly blue-shifted. TDDFT spectra show that in both **Heli** and **Heli-CF** the lowest energy absorption pertains to a degenerate process which adds both the HOMO to LUMO transition (lowest energy) and an almost isoenergetic (HOMO-1 to LUMO and HOMO to LUMO+1) one. On the contrary, in the F substituted **Heli-F2** and **Heli-CF-F2** this second transition is found at slightly higher energy (9 to 12 nm spacing) (Table 4; simulated spectra are reported in SI).

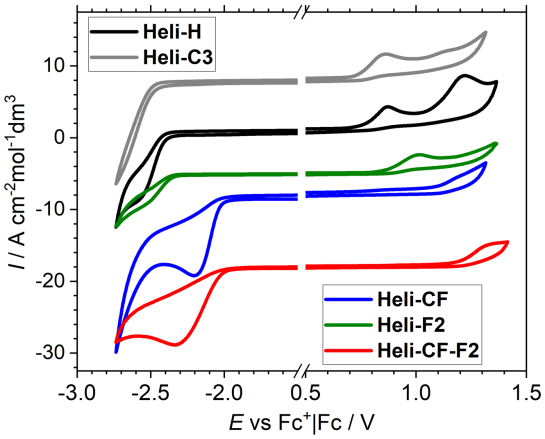

Figure 4. Synopsis of the normalized CV curves of the studied helicenes in CH_2Cl_2 solvent.

The calculated HOMO energies (table 4) significantly follow the corresponding experimental CV values (measured with the maximum criterion, table 3) whereas small positive deviations (ca. 0.15 eV) are observed in the LUMO energies of **Heli** and **Heli-F2**. **Heli-CF** as well as **Heli-CF-F2**, featuring electroreductive C-F cleavage of the perfluoro alkyl chain do not allow for similar comparison..

Table 3. Summary of redox data obtained at 0.2 V/s scan rate in CH_2Cl_2 for the fluorinated helicenes investigated in this work and benchmarks **Heli-H** and **Heli-C3**

	First reduction peak / V (Fc^+|Fc)		First oxidation Peak / V (Fc^+|Fc)		Energy levels. maxima criterion			Energy levels, onset criterion		
Compound	max	onset	onset	max	LUMO /eV	HOMO /eV	*E*g /eV	LUMO /eV	HOMO /eV	*E*g /eV
Heli-H[36]	-2.59	-2.41	0.69	0.86	-2.23	-5.68	3.45	-2.41	-5.51	3.1
Heli-C3	-2.67	-2.46	0.71	0.87	-2.13	-5.67	3.54	-2.34	-5.51	3.17
Heli-F2	-2.52	-2.34	0.82	1.01	-2.28	-5.81	3.54	-2.46	-5.62	3.17
Heli-CF	-2.20	-2.00	1.01	1.18	-2.60	-5.98	3.38	-2.81	-5.81	3.01
Heli-CF-F2	-2.32	-1.98	1.17	1.31	-2.48	-6.11	3.63	-2.83	-5.97	3.14

It is worth noting that, even without accounting for solvent interactions, calculated and experimental data practically overlap. According to both experimental and calculated frontier orbital energies, the largest electronic effects are provided by the functionalization of the 2 and 13 positions of the helicenes whereas smaller perturbations are introduced upon functionalization of the 7 and 8 positions (table 4).

Figure 5 shows the HOMO and LUMO orbital plots together with the triplet spin density (minimized triplet state) of two representative systems, **Heli-H** and **Heli-F2**. The other two terms of the group display similar orbital pattern (see supporting information). Noticing, the presence of the fluorine p-orbital in both the HOMO and LUMO of 7,8-difluoro substituted helicenes is evident although clearly do not participate in electronic delocalization.

The low energy triplet vertical transitions inferred from TDDFT calculations, lie near the onset of the phosphorescence emissions at 77K (table 4 and 2) and the pictorial representation, provided in figure 5, highlights how this surface tend to localize on the central aromatic rings of the helical framework (phenanthrene like) rather than delocalizing on a larger portion of the conjugated π-system like the HOMO and LUMO orbital. Indeed, this feature is not surprising and corroborates the finding of the high energy triplet state or, in other words, the small S_1-T_1 gap. In fact, S_1-T_1 gap depends, among other factors, on the spatial overlap (in quantum mechanics, twice the exchange integral) between singlet state and triplet states. [43]

Table 4. Lowest calculated singlet transitions (*f*, oscillator strength), HOMO and LUMO energies, and **S_0-T_1** (nm) energy gap derived from TD-DFT calculations

Compound	λ (nm) *[f]*	HOMO (eV)	LUMO (eV)	ΔE (HOMO-LUMO) (eV)	S_0-T_1 (nm)
Heli-H 0.2774D [a] B to T	384.85(0.2121) 384.70(0.0834)	-5.68	-1.99	3.69	516.3
Heli-CF 3.7959D [a] T to B	395.02(0.1900) 393.71(0.0889)	-6.05	-2.45	3.60	526.9
Heli-F2 3.3190D [a] B to T	384.63(0.2172) 375.67(0.0837)	-5.83	-2.15	3.68	518.0
Heli-CF-F2 0.7653D [a] T to B	395.34(0.1949) 383.68(0.0900)	-6.19	-2.60	3.59	529.4

[a] computed dipole moment, the dipole axe lays orthogonal to the helical C^2 symmetry axe and cross the central benzene ring passing in between the two terminal thiophene ring; the versus is herein indicated as B to T or T to B accordingly to its orientation, respectively from benzene to thiophenes or the opposite.

Comparing the two triplet surfaces in figure 5, it is evident: *i*) the different contribution of the sulphur atoms adjacent to the central benzene ring (remarkably smaller in **Heli-F2**) and *ii*) the different shapes and the presence/absence of a nodal plane on the central benzene ring. The latter characteristic leads to different distortion modes in the triplet geometries compared to the ground state ones as depicted in figure 6 (and may explain the worst resolution of the phosphorescence emission in **Heli-F2**). The former evidence (weakest contribution of the S atoms in **Heli-F2** spin density) may explain instead the origin of the lower P/F ratio observed for the two 7,8 -difluoro functionalized helicenes in terms of different efficacies of ISC/SOC.

Conclusion

Two (*E*)-1,2-difluoro-1,2 bis-(benzo[1,2b;4,3b']dithiophene)-ethenes (**Alk-F2** and **Alk-CF-F2**) have been synthesized in high yields by means of stereoconservative Stille cross coupling on (*E*)-difluorostannyl ethene. All **Alk** systems display blue fluorescence emission with QY significantly affected by the presence of fluorine atoms on the ethene bond. **Alk-F2** and **Alk-CF-F2** have been submitted to the photochemically induced oxidative cyclization achieving, in satisfactory yields, the corresponding helicenes (**Heli-F2** and **Heli-CF-F2**), therefore selectively endowing the helicene framework with two fluorine atoms on the 7,8 positions. Electrochemical and photophysical studies have been carried out and the results analysed with the aid of TDDFT calculation. With the good agreement of the compared data, structure properties correlation can be easily backed to the functionalization points (2,13 thiophene positions and 7,8 benzene ones).

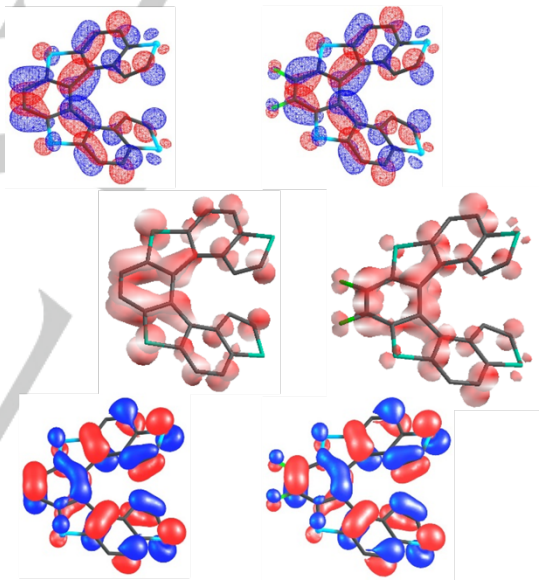

Figure 5. HOMO (bottom), LUMO (top), triplet spin density (middle) pictures of **Heli-H** (left) and **Heli-F2** (right).

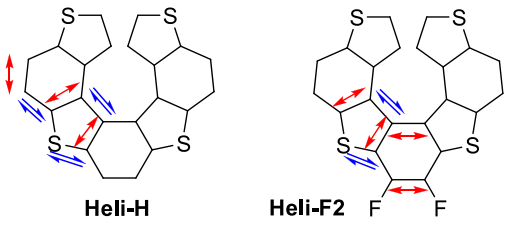

Figure 6. Summary of geometrical distortions on going from the ground state to the triplet one: bond contractions (blue arrows), bond lengthening (red arrows).

The most appealing property of thiahelicenes, that emerges from these studies, relates to their relatively high phosphorescent

emission which is found to be comparable to that of phenanthrene or benzophenanthrene. The S_1-T_1 gap in the order of 6000 cm^{-1} (like phenanthrene molecules) and the short phosphorescence radiative lifetimes, in the order of 0.1 seconds, indicate a remarkably efficient ISC dynamics of thiahelicenes with respect to the family of carbo- or aza-helicenes. It is also found, from voltammetry and optical studies as well as from DFT investigations, that the position 2,13 provide an asymmetrical electronic perturbation more effective on the LUMO whereas positions 7,8 provide more balanced perturbation on HOMO and LUMO. Theoretical studies highlights, among other features, the strong contribution of the sulphur atoms to the triplet spin density surface. Hence, low lying, sulphur *n* electrons significantly contribute to enhance ISC and reflects on the efficient phosphorescence emission. It is to note that position 7, 8 also are capable for producing larger structural distortion of excited states.

.

Experimental Section

Compounds **Alk-H**, [21c] **Alk-C3**, [21b] **Alk-CF**, [27] **Heli-C3**[21b] and **Heli-CF**[36] have been previously reported and synthesized accordingly. Unless otherwise specified, all reactions were performed under nitrogen atmosphere. All reagents and solvents were obtained from highest grade commercial sources and used without further purification. Anhydrous solvents (from Sigma-Aldrich) were purged with nitrogen before use. The reactions progress was monitored by TLC with silica gel plates and by HPLC. All chromatographic separations were carried out on Merck silica gel (60Å, 230–400 mesh). Melting points were obtained with a Büchi B-540 melting point apparatus and are uncorrected. ^{1}H NMR and ^{13}C NMR spectra were recorded on a Bruker AC300 and AMX 300 MHz spectrometers; chemical shifts (δ) are reported in parts per million with respect to the solvent residual peak. High Resolution Electron Ionization (HR-EI) mass spectra were recorded on a FISONS-Vg Autospec-M246 spectrometer. ATR FTIR were recorded as solid powder on an Shimadzu IR-Affinity 1S spectrometer with 4cm-1 resolution on a diamond crystal.

The two alkenes **Alk-F2** and **Alk-CF-F2** have been prepared by means of the Stille coupling reaction between *E*-1,2-difluoro-1,2-ditributylstannyl-ethene, **3**, and the corresponding substituted iodo-benzodithiophenes **2a** and **2b**. **Heli-F2** and **Heli-CF-F2** have been prepared from the corresponding alkene precursors by means of photochemical cyclization. **3** has been synthesized as previously reported in the literature.[54]

Synthesis of 7-tridecafluorohexyl-2-iodo-benzo[1,2b;4,3b']dithiophene (2b):

A *n*-BuLi 1.25 M solution in hexane (1.84 mL, 2.3 mmol, 1.15 eq) was added dropwise under stirring and nitrogen atmosphere to a solution of **1b** [27] (1.02 g, 2 mmol) in dry THF (12 mL) at –78 °C. The solution was stirred for 30 min at –78 °C. A solution of I_2 (1.01 g, 4.0 mmol, 2 eq) in 4 mL of dry THF was added dropwise. The progress of the reaction was monitored by TLC (light petroleum, $R_{f\ \mathbf{2a}}$ = 0.47; $R_{f\ \mathbf{20b}}$ = 0.53). After 40 min, the solution was quenched with 20 mL of aqueous solution of Na_2SO_3 and warmed to room temperature. The THF was completely removed under reduced pressure; the residue was extracted twice with 20 mL of CH_2Cl_2/Et_2O (10:1). The organic phase was dried over Na_2SO_4 and the solvent removed under reduced pressure affording 1.238 g of compound **2b** as white solid in quantitative yield. HRMS calcd for $C_{16}H_4F_{13}IS_2$: 633.85956; found: 633.85916. ^{1}H NMR (300 MHz, $CDCl_3$) δ= 7.75 (d, *J* = 8.7 Hz, 1H), 7.82 (d, *J* = 8.7 Hz, 1H), 7.93 (s, 1H), 7.98 (s, 1H) ppm. ^{13}C NMR (75MHz, $CDCl_3$) δ = 79.4 (Cq, C-I), 110.8, 115.0, 119.0 (m,Cq C-F), 118.3, 119.8, 125.1 (t, CH_8), 131.6 (CH), 130.1 (t, ^2J = 28.6 Hz, C_qCF); 131.7, 136.3, 138.4, 142.1 (Cq arom) ppm; ^{19}F NMR (282.23 MHz, $CDCl_3$) δ= –81.1 (s, 3F), –102.1 (s, 2F), –121.7 (s, 4F), –123.1 (s, 2F), –126.4 (s, 2F); MS (EI): *m/z* (%) = 634 (M^+,95), 507 ([M-I]$^+$, 15), 365 ([M-(C_5F_{11})]$^+$, 100), 238 ([M-(I+(C_5F_{11})]$^+$, 45).

General procedure for the coupling with stannane 3: [29]

To a stirred solution of (*E*)-(1,2-difluoro-1,2-ethenediyl)-bis-tributylstannane **3** (0.5 eq) and halides **2a, b** (1.01 eq) in 4 mL/mmol of THF/DMF solvent mixture (1/1 v/v), 0.5 eq. of CuI and 0.05 eq. of $Pd(PPh_3)_4$ (5 mol %) were added at room temperature. The reaction resulted to be exothermic and the stirred mixture quickly turned into a yellow-brown suspension. The progress of the reaction was monitored by TLC (light petroleum/CH_2Cl_2, 8:2) and ^{19}F NMR analysis was employed to follow disappearing of the reactant **3**. After stirring for 3 h, the ^{19}F NMR chemical shift of the (*E*)-(1,2-difluoro-1,2-ethenediyl) bis [tributylstannane] (δ_3 = –159.1 ppm) [29] had disappeared and a new singlet was observed. The reaction mixture was diluted with 60 mL/mmol of THF/Et_2O/CH_2Cl_2 5:3:1 and treated with 20 mL of 10% aqueous NH_3; the organic phase was then washed with brine and water and then the solvent removed under reduced pressure. The residue was washed several times with *n*-hexane and centrifuged to afford the target compounds.

Alk-F2: Yield= 83%. HRMS calcd for $C_{22}H_{10}F_2S_4$: 439.96334; found: 439.96262; subl. 226-228 °C. ^{1}H NMR (300 MHz, $CDCl_3$) δ = 7.62 (d, *J* = 5.4 Hz, 2H), 7.76 (d, *J* = 5.4 Hz, 2H), 7.80 (d, *J* = 8.6 Hz, 2H), 7.87 (d, *J* = 8.6 Hz, 2H), 8.04 (s, 1H) ppm. ^{1}H NMR (300 MHz, THF-d8) δ = 7.76 (d, *J* = 5.4 Hz, 2H), 7.88 (d, *J* = 8.7 Hz, 2H), 7.92 (d, *J* = 5.4 Hz, 2H), 7.94 (d, *J* = 8.7 Hz, 2H), 8.20 (s, 1H) ppm ^{13}C NMR (75MHz, THF-d8) δ = 119.0, 121.2, 121.6, 123.0, 128.3 (Cq arom) ppm; ^{19}F NMR (282.23 MHz, THF-d_8) δ = –142.2 (s, 2F, =CF) MS (EI): *m/z* (%) = 440 (M^+,100), 220 ([M/2]$^+$, 25).

Alk-CF-F2: Yield= 84%. HRMS calcd for $C_{34}H_8F_{28}S_4$: 1075.90618; found: 1075.90730; mp 161-163 °C. ^{1}H NMR (300 MHz, $CDCl_3$) δ= 7.75 (d, *J* = 8.7 Hz, 1H), 7.82 (d, *J* = 8.7 Hz, 1H), 7.93 (s, 1H), 7.98 (s, 1H) ppm. ^{13}C NMR (75MHz, $CDCl_3$) δ = 79.4 (Cq, C-I), 110.8, 115.0, 119.0 (m,Cq C-F), 118.3, 119.8, 125.1 (t, CH_8), 131.6 (CH), 130.1 (t, ^2J = 28.6 Hz, C_qCF); 131.7, 136.3, 138.4, 142.1 (Cq arom) ppm; ^{19}F NMR (282.23 MHz, $CDCl_3$) δ = -81.1 (s, 6F), -102.05 (s, 4F), -121.7 (s, 8F), -123.1 (s, 4F), -126.45 (s, 4F); – 143.8 (s, 2F, =CF) MS (EI): *m/z* (%) = 1076 (M^+,100), 807 ([M-C_5F_{11}]$^+$, 15).

Photocyclization to helicenes, general procedure:

In a 250 mL photoreactor, equipped with a quartz jacket, cooled immersion medium pressure 125W Hg lamp, the alkene was dissolved or suspended in benzene and a catalytic amount of PhSSPh was added. While bubbling air into the solution, the reaction was irradiated. After complete conversion of the starting material, the solution was washed with an aqueous Na_2SO_3 solution. The organic layer was dried over Na_2SO_4 and the solvent removed under reduced pressure. The crude was purified by means of column chromatography on silica gel, with *n*-hexane as the eluent, affording the proper **Heli**.

Heli-F2: Reaction time, 9 hours, Yield, 23%; HRMS calcd for $C_{22}H_8F_2S_4$: 437.94769; found: 437.94669. ^{1}H NMR (300 MHz, $CDCl_3$) δ= 8.05 (d, *J* = 8.5 Hz, 2H), 7.96 (d, *J* = 8.5 Hz, 2H), 6.93 (d, *J*=5.6 Hz, 2H), 6.70 (d, *J*= 5.6 Hz, 2H) ppm. ^{13}C NMR (75MHz, $CDCl_3$) δ = 119.0, 122.1, 125.3, 125.4 (CH arom); 127.8, 130.7, 136.4, 137.3, 137.6 (Cq arom); 143.2 (dd, C-F, $^1J_{C\text{-}F}$ = 249.1Hz $^2J_{C\text{-}C\text{-}F}$ =15.9 Hz). ^{19}F NMR (282.23 MHz, $CDCl_3$) δ = –143.4 (s, 2F, =C-F) MS (EI): *m/z* (%) = 438 (M^+,100).

Heli-CF-F2: Reaction time, 8 hours, Yield: 30%. HRMS calcd for $C_{34}H_6F_{28}S_4$: 1073.89053; found: 1073.89280. ^{1}H NMR (300 MHz, $CDCl_3$) δ= 8.13 (d, *J* = 8.7 Hz, 2H), 8.08 (d, *J* = 8.7 Hz, 2H), 7.06 (s, 2H) ppm. ^{13}C NMR (75MHz, $CDCl_3$) δ = 111.0, 115.0, 119.0 (m,Cq C-F); 121.9, 121.9, 127.7 (CH_{arom}), 127.0, 130.7, 134.2, 138.4, 139.5 (Cq arom); 143.7 (dd, C-F, $^1J_{C\text{-}F}$ = 294.7 Hz, $^2J_{C\text{-}C\text{-}F}$ =15.4 Hz) ppm; ^{19}F NMR (282.23 MHz,

$CDCl_3$) δ = –81.2 (s, 6F), –102.9 (s, 4F), –121.8 (s, 8F), –123.3 (s, 4F), –126.5 (s, 4F); – 142.0 (s, 2F, =C-F) MS (EI): *m/z* (%) = 1074 (M^+,100).

Optical spectroscopy: UV-visible spectra were measured with a Hewlett-Packard 4853 diode array spectrophotometer. Steady-state emission spectra were measured using a Photon Technology International QuantaMaster model C-60 spectrofluorimeter, correcting them for the photodetector response. Phosphorescence lifetime measurements were performed using the same fluorimeter equipped with a microsecond xenon flash lamp or using an IBH Fluorocube fluorimeter, equipped with a blue LED (λ_{max} = 405 nm) by time-correlated single-photon counting. Nanosecond lifetimes were measured by TCSPC methods on an Edinburgh FS980 equipped with a 375 pulsed laser. Lifetimes were fitted with multiexponential decay curves and average lifetime was calculated according to $\boldsymbol{\tau_{av}} = \sum_{n=1}^{m} \alpha_n \tau_n^2 / \sum_{n=1}^{m} \alpha_n \tau_n$, where *m* is the *nth* component of the fitted decay and *a* is the pre-exponential value of the *nth* component.

Luminescence quantum efficiencies (QE) were measured using a Hamamatsu C9920 system equipped with a xenon lamp, calibrated integrating sphere and C10027 photonic multichannel analyser. The QE measurements were carried out at room temperature in dichloromethane (CH_2Cl_2) solutions. Low temperature measurements were performed in 2-MeTHF frozen glass at 77K; 2% (wt/wt, 100mg/mL PMMA) PMMA doped film were spincoated onto a quartz substrate and the emission spectra recorded at room temperature, in both air and nitrogen filled atmosphere (or hgh vacuum evacuated Schlenk tube), as well as at 77K.

Cyclovoltammetric studies: Fluorinated tetrathiahelicenes **Heli-CF**, **Heli-F2** and **Heli-CF-F2**, precursor **Alk-CF** and tetrathiahelicene **Heli-C3** (included as non-fluorinated reference) were characterized by cyclic voltammetry, CV, at potential scan rates ranging from 0.05 to 5 V/s, at concentrations ranging 0.00025-0.001 M in both CH_2Cl_2 and ACN (in some cases 1 : 4 ACN + toluene mixed solvent) with 0.1 M tetraethylammonium perchlorate TBAP as the supporting electrolyte, deaerated by N_2 purging. The ohmic potential drop was compensated by the positive feedback technique. The experiments were carried out using an AUTOLAB PGSTAT potentiostat of EcoChemie (Utrecht, The Netherlands) run by a PC with the GPES 4.9 software of the same manufacturer. The working electrode was a glassy carbon GC disk embedded in Teflon® (Amel, 0.071 cm^2); the counter electrode was a platinum wire. The operating reference electrode was an aqueous saturated calomelane (SCE) having a potential of -0.485 V (CH_2Cl_2), -0.39 V (ACN), and -0.495 V (ACN+toluene 1 : 4) *vs* that of the Fc^+|Fc couple (the intersolvental redox potential reference currently recommended by IUPAC).[55] The optimised polishing procedure for the working disk electrodes consisted in surface treatment with a synthetic diamond powder of 1 mm in diameter of Aldrich on a DP-Nap wet cloth of Struers. Electrochemical polymerization ability was tested by repeated CV cycling in the potential range of the first anodic peak at 0.2 V/s potential scan rate, followed, in case of film deposition, by CV stability tests consisting in repeated cycling in monomer-free solution.

Theoretical calculations: DFT and TD-DFT calculations were performed on the **Alk** systems as well as on their **Heli** derivatives with the Gaussian09[54] computational package. For computational purposes propyl chain in **Heli-C3** were replaced by hydrogen atoms and the perfluorohexyl chains in **Heli-CF**. **Heli CF-F2**, **Alk-CF** and **Alk-CF-F2** were replaced with simple -CF_3 group. Ground state geometries have been optimized at the DFT B3LYP/6-31G* theory level; [51] the first six singlet and triplet transitions have been calculated by the TDDFT B3LYP/6-311G* from the optimised ground state geometry; HOMO and LUMO energy levels are reported from the B3LYP/6-311G* calculations. Triplet state geometry optimisations employed the unrestricted version of the B3LYP/6-31G* formalism starting from the minimized singlet ground state structures. Chemcraft computational suite (www.chemraftprog.com) was employed to render HOMO and LUMO orbitals and TD spectra.

The data that support the finding of this study are available in the supporting material of this article.

Acknowledgements

The University of Milan for the Post Doctorate fellowship to AB. AB thanks Prof. Stefano Maiorana for mentoring and for the fruitful discussions. This study was supported by Regione Lombardia and Fondazione CARIPLO (grant numbers 12689/13, 7959/13; Azione 1 e 2, “SmartMatLab centre”), the Italian MUR under the project PRIN 2017 (grant no. 2017FJCPEX “3DFARE: Functional 3D architectures for electrochemiluminescence applications”). The authors thank Fondazione “Banca del Monte di Lombardia” for the funding of the LCMS2020 mass spectrometer.

Keywords: tetrathia[7]helicene • Photophysics • Triplet state • Cyclic voltammetry • Fluorinated helicenes

References

[1] M. Nakano, H. Mori, S. Shinamura, K. Takimiya, *Chem. Mater.* **2012,** *24*, 190−198

[2] a) H. Yersin, in *Highly Efficient OLEDs with Phosphorescent Materials*, Wiley, Weinheim, Germany **2018**; L. R. Dalton, P. A. Sullivan, D. H. Bale, *Chem. Rev.* **2010**, *110*, 25-55; b) G. S. He, L-S. Tan, Q. Zheng, P. N. Prasad, *Chem. Rev.* **2008**, *108*, 1245-1330; c) M. E. Thompson, P. E. Djurovich, S. Barlow, S. Marder, in *Comprehensive Organometallic Chemistry III,* Vol 12 (Eds: R. H. Crabtree, D. M. P. Mingos), Elsevier **2007,** Ch. 4.

[3] a) M. Muccini, S. Toffanin, in *Organic Light-Emitting Transistors: Towards the Next Generation Display Technology*, Wiley, Hoboken, NJ, USA **2016**; b) Y. Shirota, H. Kageyama, *Chem Rev.* **2007**, *107*, 953-1010; c) J. E. Anthony, *Chem. Rev.* **2006,** *106*, 5028−5048; d) J. E. Anthony, *Angew. Chem., Int. Ed.* **2008,** *47*, 452−483; e) K. Takimiya, S. Shinamura, I. Osaka, E. Miyazaki, *Adv. Mater.* **2011,** *23*, 4347−4370.

[4] a) J. Chen, Y. Cao, *Acc. Chem. Res.* **2009**, *42(11)*, 1709-1718; b) S. Yoo, B. Domercq, B. Kippelen, *Appl. Phys. Lett.* **2004**, *85*, 5427−5429; c) M. Y. Lloyd, A. C. Mayer, S. Subramanian, D. A. Mourey, D. J. Herman, A. V. Bapat, J. E. Anthony, G. G. Malliaras, *J. Am. Chem. Soc.* **2007,** *129*, 9144−9149; d) J. Yang, T.-Q. Nguyen, *Org. Electron.* **2007,** *8*, 566−574; e) D. Kotowski, S. Luzzati, F. Bertini, M. Cavazzini, S. Orlandi, A. Bossi, M. Catellani, E. Kozma, *Mater. Chem. Phys.* **2015**, *63*, 152-160.

[5] F. J. M. Hoeben, P. Jonkheijm, E. W. Meijer, A. P. H. J. Schenning, *Chem. Rev.* **2005**, *105*, 1491-1546.

[6] a) Y. Shen, C.-F. Chen, *Chem. Rev.* **2011,** *112 (3)*, 1463–1535 and ref. 1 and 2; b) Y. Shen, C.-F. Chen, *Chem. Rev.* **2012**, *112*, 1463–1535; Applications: Marc Gingras, *Chem. Soc. Rev.* **2013,** *42*, 1051-1095.

[7] C.-F. Chen, Y. Shen, Y. in *Helicene Chemistry, from Synthesis to Applications*; Springer, Berlin/Heidelberg, Germany, **2017**.

[8] Y. Nakai, T. Mori, Y. Inoue, *J. Phys. Chem. A* **2012**, *116*, 7372–7385.

[9] W.-L. Zhao, M. Li, H.-Y.Lu, C.-F. Chen, *Chem. Commun.* **2019**, *55*, 13793–13803.

[10] P. Aillard, A. Voituriez, A. Marinetti, *Dalton Trans.* **2014**, *43*, 15263–15278.

[11] R. Amemiya, M. Yamaguchi, *Org. Biomol. Chem.* **2008**, *6*, 26–35.

[12] Y. Xu, Y. X. Zhang, H. Sugiyama, T. Umano, H. Osuga, K. Tanaka, *J. Am. Chem. Soc.* **2004**, *126*, 6566–6567.

[13] H. Nakagawa, K. Gomi, K.-I. Yamada, *Chem. Pharm. Bull.* **2001**, *49*, 49–53.

[14] S. Arnaboldi, S. Cauteruccio, S. Grecchi, T. Benincori, M. Marcaccio, A. O. Biroli, G. Longhi, E. Licandro, P. R. Mussini, *Chem. Sci.* **2019**, *10*, 1539–1548.

[15] Gingras, M. One hundred years of helicene chemistry. Part 3: Applications and properties of carbohelicenes. Chem. Soc. Rev. 2013, 42, 1051–1095.

[16] Y. Yang, R. da Costa, M. Fuchter, A. J. Campbell, *Nat. Photonics*. **2013**, *7*, 634-638.

[17] a) E. Licandro, S. Cauteruccio, D. Dova, *Adv. Heteroc. Chem.* **2016**, *118*, 1–46; b) S. K. Collins, M. P. Vachon, *Org. Biomol. Chem.* **2006**, *4*, 2518–2524.

[18] a) I. Stary, I. G. Stara, *Targets in Heterocyclic Systems* **2017**, *21*, 23–53; b) F. Dumitrascu, D. G. Dumitrescu, I. Aron, Arkivoc **2010**, *i*, 1–32.

[19] a) K. Dhbaibi, L. Favereau, J. Crassous, *Chem. Rev.* **2019**, *119*, 8846–8953; b) F. Pop, N. Zigon, N. Avarvari, *Chem. Rev.* **2019**, *119*, 8435–8478; c) L. Zhou, H. Liu, J. Tan, C. Liu, X.-Y. Cao, A. Narita, Y. Hu, *Chem Asian J.* **2022**, *17*, e202200336.

[20] a) D. Dova, S. Cauteruccio, S. Prager, A. Dreuw, C. Graiff, E. Licandro, *J. Org. Chem.* **2015**, *80*, 3921–3928; b) A. Bossi, S. Maiorana, C. Graiff, A. Tiripicchio, E. Licandro, *Eur. J. Org. Chem.* **2007**, 4499–4509; c) K. Tanaka, H. Osuga, K. Kitahara, *J. Org. Chem.* **2002**, *67(6)*, 1795-1801; d) K. Tanaka, H. Osuga, Y. Kitahara, *J. Chem. Soc., Perkin Trans. 2* **2000**, 2492-2497; e) K. Tanaka, Y. Kitahara, *Chem. Commun.* **1998**, 1141-1142.

[21] a) C. Rigamonti, M. T. Ticozzelli, A. Bossi, E. Licandro, C. Giannini, S. Maiorana, *Heterocycles* **2008**, 76, 1439-1470; b) E. Licandro, C. Rigamonti, M. T. Ticozzelli, M. Monteforte, C. Baldoli, C. Giannini, S. Maiorana, *Synthesis* **2006**, 3670-3678; c) S. Maiorana, A. Papagni, E. Licandro, R. Annunziata, P. Paravidino, D. Perdicchia, C. Giannini, M. Bencini, K. Clays, A. Persoons, *Tetrahedron* **2003**, *59*, 6481-6488; d) F. Fenili, A. Bossi, E.Licandro, P. Ferruti, E. Ranucci, A. Manfredi, C. Baldoli, S. Cauteruccio, E. Licandro, E. Ranucci, *J. Pol. Sci A: Polymer Chemistry*, **2010,** 48, 4704–4710.

[22] a) A. Facchetti, M.-H Yoon, G. R. Hutchison, C. L. Stern, M. A. Ratner, T. J. Marks, *J. Am. Chem. Soc.* **2004**, *126*, 13480-13501; b) A. Facchetti, M. Mushrush, M.-H. Yoon, G. R. Hutchison, M. A. Ratner, T. J. Marks, *J. Am. Chem. Soc.* **2004**, *126*, 13859-13874.

[23] a) R. Ragni, A. Punzi, F. Babudri, G. M. Farinola, *Eur. J. of Org. Chem.*, **2018**, *27*, 3500-3519; b) A. Cardone, C. Martinelli, F. Babudri, F. Naso, V. Pinto, G. M. Farinola, *Current Organic Synthesis,* **2012**, *9*, 150-162.

[24] M. Shimizu, T. Hiyama, *Angew. Chem. Int. Ed.* **2005**, *44*, 214 – 231. tematic issue, *Chem. Rev.*, **1996**, *96(5)*, 1555-1824.

[25] M. Pagliaro, R. Ciriminna, *J. Mater. Chem.*, **2005**, *15*, 4981–4991.

[26] D. O'Hagan, *Chem. Soc. Rev.* **2008**, *37*, 308–319.

[27] a) C. Kim, T. J. Marks, A. Facchetti, M. Schiavo, A. Bossi, S. Maiorana, E. Licandro, F. Todescato, S. Toffanin, M. Muccini, C. Graiff, A. Tiripicchio, *Organic Electronics,* **2009**, *10*, 1511-1520; b) U. Giovannella, C. Botta, A. Bossi, E. Licandro, S. Maiorana, *J. Appl. Phys.*, **2006**, 100, 083107.

[28] C. Baldoli, A. Bossi, C. Giannini, E. Licandro, S. Maiorana, D. Perdicchia, M. Schiavo, *SynLett*, **2005**, *7*, 1137-1141.

[29] F. Babudri, A. Cardone, L. De Cola, G. M. Farinola, G. K. Kottas, C. Martinelli, F. Naso, *Synthesis* **2008**, *10,* 1580-1588. Q. Liu, D. J. Burton, *Org. Lett.* **2002**, *4(9)*, 1483-1485.

[30] F. B. Mallory, C. W. Mallory, *Organic Reactions, Photocyclization of Stilbenes and Related Molecules*, Vol 30, (Ed. W. G. Dauben), J. Wiley & Son **1984**, 1-151.

[31] Y. Patehebieke, *Beilstein J. Org. Chem.* **2020**, *16*, 1418–1435.

[32] a) M. B. Groen, H. Schadenberg, H. Wynberg, *J. Org. Chem.* **1971**, *36*, 2797-2809 and references therein; b) J. Larsen, K. Bechgaard, *Acta Chem. Scand.* **1996**, *50*, 83-89.

[33] a) N. C. Craig, E. A. Entemann, *J. Am. Chem. Soc.* **1961**, *83*, 3047-3050; b) H. Goerner, *J. Photoch. Photobiol. A*, **1995**, *90(1)*, 57-63.

[34] A. Bolzoni, L. Viglianti, A. Bossi, S. Cauteruccio, P. R. Mussini, C. Baldoli, E. Licandro, *Eur. J. Org. Chem.* **2013**, *33*, 7489-7499.

[35] a) P. Gajdek, R. S. Becker, F. Elisei, U. Mazzucato, A. Spalletti, *J. Photochem. Photobiol. A: Chemistry* **1996**, *100*, 57-64; b) G. Bartocci, G. Galiazzo, G. Ginocchietti, U. Mazzucato, A. Spalletti, *Photochem. Photobiol. Sci.* **2004**, *3*, 870 – 877.

[36] A. Bossi, L. Falciola, C. Graiff, S. Maiorana, C. Rigamonti, A. Tiripicchio, E. Licandro, P. R. Mussini, *Electrochimica Acta,* **2009**, *54(22),* 5083-5097.

[37] A. Pietrangelo, B. O. Patrick, M. J. MacLachlan, M. O. Wolf, *J. Org. Chem.* **2009**, *74*, 4918–4926.

[38] J. B. Birks, D. J. S. Birch, *Chem. Phys. Lett*. **1976**, *43(1)*, 33-36.

[39] a) M. Sapir, E. Van der Donckt, *Chem. Phys. Lett*. **1975**, *36(1)*, 108-110; b) K. H. Grellmann, P. Hentzschel, T. Wismontski-Knittel, E. Fisher, *J. Photochemistry*, **1979**, *11*, 197-213.

[40] S. Cauteruccio, A. Loos, A. Bossi, M. C. Blanco Jaimes, D. Dova, F. Rominger, E. Licandro, A. S. K. Hashmi, *Inorg. Chem.* **2013**, *52(14),* 7995–8004.

[41] Considerations on higher states couplings are reported in: M. F. O'Dwyer, M. A. El-Bayoumi, S. J. Strikler, *J. Chem. Phys,* **1962**, *36(5)*, 1395-1396.

[42] M. Sapir, E. V. Donckt, *Chem. Phys. Lett*. **1975**, *36*, 108–110; K. Schmidt, S. Brovelli, V. Coropceanu, D. Beljonne, J. Cornil, C. Bazzini, T. Caronna, R. Tubino, F. Meinardi, Z. Shuai, J.-L. Bredas, *J. Phys. Chem. A*, **2007**, *111*, 10490-10499.

[43] N.J. Turro, *Modern Molecular Photochemistry*, University Science Books, Sausalito, CA, **1991**

[44] a) T. Azumi, S. P. McGlynn, *J. Chem. Phys.* **1962**, *37*, 2413-2420; b) H. B. Klevens, J. R. Platt, *J. Chem. Phys.* **1949**, *17(5)*, 470-481.

[45] K. Dhbaibi, P. Morgante, N. Vanthuyne, J. Autschbach, L. Favereau, J. Crassous, *J. Phys. Chem. Lett.* **2023**, *14*, 1073−1081; K. Schmidt, S. Brovelli, V. Coropceanu, J.-L. Bredas, C. Bazzini, T. Caronna, R. Tubino, F. Meinardi, *J. Phys. Chem. A*, **2006**, *110*, 11018-11024; C. Shen, M. Srebro-Hooper, M. Jean, N. Vanthuyne, L. Toupet, J. A. G. Williams, A. R. Torres, A. J. Riives, G. Muller, J. Autschbach, J. Crassous, *Chem. Eur. J.* **2017**, *23*, 407−418; K. Nagarajan, A. R. Mallia, K. Muraleedharan, M. Hariharan, *Chem. Sci.* **2017**, *8*, 1776−1782.

[46] W. Rhodes, M. F. A. El-Sayed, *J. Mol. Spectrosc.* **1962**, *9*, 42-49.

[47] S. P. McGlynn, T. Azumi, M. Kinoshita, M. "Molecular spectroscopy of the triplet state", Chapter 3, Ed. Prentice-hall, Inc. Englewood Cliffs, New Jersey **1969**.

[48] C. Hansch, A. Leo, R.W. Taft, *Chem. Rev.* **1991**, *91*, 165-195.

[49] K. Uneyama, G. Mizutani, K. Maeda, T. Kato, *J. Org. Chem.* **1999**, *64*, 6717-6723.

[50] J. A. Marsella, A. G. Gilicinski, A. M. Coughlin, G. P. Pez, *J. Org. Chem.* **1992,** *57*, 2856-2860; A. A. Pud, G. S. Shapoval, V. P. Kukhar, O. E. Mikulina, L.L. Gervits, *Electrochimica Acta* **1995**, *40(9)*, 1157-1164.

[51] A. Bossi, E. Licandro, S. Maiorana, C. Rigamonti, S. Righetto, G.R. Stephenson, M. Spassova, E. Botek, B. Champagne, *J.Phys Chem. C.* **2008**, *112(21)*, 7900-7907.

[52] In general theoretical excitation transitions are often smaller than the experimental ones due to different origins including absence of vibronic structures and limitations of the TDDFT scheme: a) Bauernschmitt, R.; Ahlrichs, R. *Chem. Phys. Lett.* **1996**, *256*, 454; b) Stratmann, R. E.; Scuseria, G.; Frisch, M. J. *J. Chem. Phys.* **1998**, *109*, 8218; c) Schipper, P. R. T.; Gritsenko, O. V.; van Gisbergen, S. J. A.; Baerends, E. J. *J. Chem. Phys.* **2000,** *112*, 1344; (a) A. Masunov, S. Tretiak, *J. Phys. Chem. B* **2004,** *108*, 899; d) F. C. Grozema, P. Th. van Duijnen, L. D. A. Siebbeles, A. Goossens, S. W. de Leeuw, *J. Phys. Chem. B* **2004,** *108*, 16139; e) D. Rappoport, F. Furche, *J. Am. Chem. Soc.* **2004,** *126*, 1277; f) M. Guillaume, B. Champagne, F. Zutterman, *J. Phys. Chem. A* **2006,** *110*, 13007.

[53] F. Babudri, A. Cardone, G. M. Farinola, C. Martinelli, R. Mendichi, F. Naso, M. Striccoli *Eur. J. Org. Chem.* **2008**, 1977-1982.

[54] G. Gritzner, J. Kuta, *Pure Appl. Chem.* **1984**, *56*, 461-466; G. Gritzner, *Pure Appl. Chem.* **1990**, *62,*1839-1858.

[55] Gaussian 09, Revision C.01. M. J. Frisch, G. W. Trucks, H. B. Schlegel, G. E. Scuseria, M. A. Robb, J. R. Cheeseman, G. Scalmani, V. Barone, B. Mennucci, G. A. Petersson, H. Nakatsuji, M. Caricato, X. Li, H. P. Hratchian, A. F. Izmaylov, J. Bloino, G. Zheng, J. L. Sonnenberg, M. Hada, M. Ehara, K. Toyota, R. Fukuda, J. Hasegawa, M. Ishida, T. Nakajima, Y. Honda, O. Kitao, H. Nakai, T. Vreven, J. A. Montgomery, Jr., J. E. Peralta, F. Ogliaro, M. Bearpark, J. J. Heyd, E. Brothers, K. N. Kudin, V. N. Staroverov, T. Keith, R. Kobayashi, J. Normand, K. Raghavachari, A. Rendell, J. C. Burant, S. S. Iyengar, J. Tomasi, M. Cossi, N. Rega, J. M. Millam, M. Klene, J. E. Knox, J. B. Cross, V. Bakken, C. Adamo, J. Jaramillo, R. Gomperts, R. E. Stratmann, O. Yazyev, A. J. Austin, R. Cammi, C. Pomelli, J. W. Ochterski, R. L. Martin, K. Morokuma, V. G. Zakrzewski, G. A. Voth, P. Salvador, J. J. Dannenberg, S. Dapprich, A. D. Daniels, O. Farkas, J. B. Foresman, J. V. Ortiz, J. Cioslowski, and D. J. Fox, Gaussian, Inc., Wallingford CT, 2010;

Entry for the Table of Contents

Insert graphic for Table of Contents here.

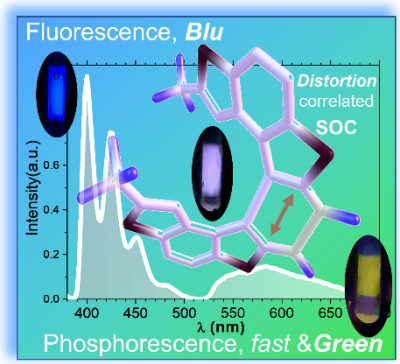

Fluorination of tetrathia[7]helicene backbone disclosed important functionalization related structure-electronic alterations in perspective important in the design of novel chiral derivatives. [7]THs also show brilliant green phosphorescence resulting from enhanced SOC due to S-atom effect and distortion-annulation.

Institute and/or researcher Twitter usernames: